



Cite this: *Nanoscale*, 2018, **10**, 6060

Near ultra-violet to mid-visible band gap tuning of mixed cation $\text{Rb}_x\text{Cs}_{1-x}\text{PbX}_3$ ($X = \text{Cl}$ or Br) perovskite nanoparticles†

Daniel Amgar, Tal Binyamin, Vladimir Uvarov and Lioz Etgar *

One of the most attractive features of perovskite materials is their chemical flexibility. Due to innovative chemical compositions of perovskites, their optical and structural properties, and functionalities have become more advanced, enabling better solar performance in photovoltaics, as well as robustness and excellent properties in the nanoscale for optoelectronics. The quest for novel perovskite compositions in the nano-scale is significantly important. This paper reports on a mixed-cation system of $\text{Rb}_x\text{Cs}_{1-x}\text{PbX}_3$ (where $X = \text{Cl}$ or Br) nanoparticles. The absorption of the nanoparticles is tunable in the near ultra-violet and visible regions between ~ 395 – 525 nm for $\text{Rb}_x\text{Cs}_{1-x}\text{PbX}_3$ ($x = 0$ to $x = 0.8$ and $X = \text{Cl}$ or Br). The photoluminescence quantum yields (PLQY) of the mixed Rb^+/Cs^+ nanoparticle systems are comparable to the PLQY of CsPbX_3 nanoparticles. Interestingly an attempt to synthesize Cl^- and Br^- -based nanoparticles with high Rb^+ content was successful, although possessing low tolerance factors. We conclude that these mixed Rb^+/Cs^+ nanoparticles are more adjustable to structural distortions caused by cation substitutions than their bulk counterparts, which opens a way towards the development of more advanced mixed-ion perovskite compositions in the nano-scale.

Received 24th December 2017,
Accepted 18th February 2018

DOI: 10.1039/c7nr09607k

rsc.li/nanoscale

Introduction

Lead halide perovskite materials have been intensively studied during the past few years for their outstanding photovoltaic activity. The formula that defines the perovskite is AMX_3 and it enables high diversity, from organic–inorganic hybrids to all-inorganic perovskites, mostly as methylammonium lead halide (MAPbX_3 ; $X = \text{Cl}$, Br , I) or cesium lead halide (CsPbX_3 ; $X = \text{Cl}$, Br , I) compositions. The diverse nature of perovskites has encouraged the investigation of advanced perovskite materials using chemical modifications. A lot of reports have focused on the substitution of the monovalent cation [$A = \text{methylammonium (MA) CH}_3\text{NH}_3$, formamidinium (FA) $\text{CH}_3(\text{NH}_2)_2$, or Cs^+], the divalent metal cation ($M = \text{Pb}^{2+}$, Sn^{2+} and Ge^{2+}), and the halide ($X = \text{Cl}^-$, Br^- or I^-).^{1–13} Chemical modifications for perovskites are of great importance, enabling band-gap engineering, adjustment of properties for specific requirements, refraining from the use of toxic compounds, improvements of the synthetic routes, enhancing product quality, and so on. In the field of solar energy, the most efficient perovs-

kite-based solar cell was fabricated with a mixed-cation perovskite composition, reaching 22.1%, which emphasizes the importance of chemically modified perovskites.^{14,15} Apart from bulk perovskites, mixed-halide systems in the nano-scale are being thoroughly investigated,^{16–18} while mixed-cation systems are still behind for both hybrid organic–inorganic and all-inorganic perovskite nanoparticles (NPs). Recently, the mixed-cation system was applied for NPs by Protesescu *et al.* who reported on FAPbI_3 and $(\text{FA/Cs})\text{PbI}_3$ perovskite NPs with improved robustness, relative to MA - or Cs -based perovskite NPs, and emissions in the near-infrared spectral region.¹⁹ Moreover, Liu *et al.* proposed a mixed-metal cation system of $\text{CsPb}_x\text{Mn}_{1-x}\text{Cl}_3$ and revealed a new perspective for tuning the optical properties of perovskite NPs.⁹

The optical properties of perovskite NPs are mainly affected by their electronic structure, while structural distortions are known to influence them as well. By considering the specific geometry required for an ideal perovskite, only a specific combination of ions will be suitable. The Goldschmidt tolerance factor (TF) is aimed at predicting a stable perovskite structure, related to a 3D-cubic close packing of ions.^{20–22} For an ideal cubic structure the TF is calculated as follows: $t = (r_A + r_X)/\sqrt{2}(r_M + r_X)$, where r is the ionic radius, and the empirical formability range is $0.8 < t < 1.0$.²³ Considering the TF restrictions, most of the monovalent elemental cations are mismatched to establish a stable perovskite. Recently, the rubi-

The Institute of Chemistry, The Center for Nanoscience and Nanotechnology, The Casali Center for Applied Chemistry, The Hebrew University of Jerusalem, Jerusalem, Israel. E-mail: lioz.etgar@mail.huji.ac.il

† Electronic supplementary information (ESI) available: Absorption, XRD analysis and EDS elemental analysis. See DOI: 10.1039/c7nr09607k

dium cation (Rb^+) was suggested to balance the TF for a better solar efficiency and better perovskite stability due to its non-oxidative nature.¹² Another work by Linaburg *et al.* describes solid solutions of inorganic mixed-cation $\text{Cs}_{1-x}\text{Rb}_x\text{PbX}_3$ ($X = \text{Cl}$ or Br) perovskites showing the adjustable nature of perovskites, and exploring their structural and optical response to changes in the TF. This gave a new insight into the lower limit of the TF for which perovskites remain stable at room temperature.¹³

Nonetheless mixed-cation systems have been studied in the bulk form, and mixed-cation perovskites in the nano-scale remain poorly explored. In general, small perovskite NPs are known to adjust their strain distribution and lattice parameters, compared with the bulk form. Therefore, the structural flexibility of perovskite NPs to A-cation substitutions, full or partial, is assumed to be different in the nano-scale due to a more adjustable nature of the contraction and expansion of the structure.^{19,24} RbPbCl_3 and RbPbBr_3 compositions are yet to be successfully synthesized due to the small Rb^+ cation, and relatively small TF values of 0.806 and 0.801, respectively. Motivated by the structural suppleness and the option to achieve higher TFs by mixing different cations, we successfully synthesized Rb^+/Cs^+ -based lead halide perovskite NPs with a tunable composition of $\text{Rb}_x\text{Cs}_{1-x}\text{PbX}_3$ ($x = 0, 0.2, 0.6, 0.8$; $X = \text{Cl}, \text{Br}$). Characterization studies revealed new insights regarding the crystal structure and the degree of flexibility of the octahedral PbX_6 network while the optical properties were tuned based on the Rb^+/Cs^+ ratio. The NPs exhibit photoluminescence quantum yields (PLQY) of up to $\sim 60\%$, tunable emissions in the visible region, and intriguing structural changes upon increasing the Rb^+ content in the crystal. The results show an approximated upper limit of $x = 0.8$ for $\text{Rb}_x\text{Cs}_{1-x}\text{PbX}_3$ yielding absorption peaks, which are blue shifted compared with CsPbX_3 NPs. For the nominal $x = 1$ Cl-based NPs, a structural change in the $\text{Rb}_6\text{Pb}_5\text{Cl}_{16}$ phase was observed and explored in our recently published work.²⁵ In the case of $x = 1$ for Br-based NPs, the NPs failed to form. Energy dispersive X-ray spectroscopy (EDS) and absorption measurements of control experiments without Rb confirmed the presence of Rb^+ in the NPs.

Results and discussion

Fig. 1 presents the calculations of the TFs of several perovskite compositions. In the x -axis, increasing Rb^+ content ($\text{Rb}^+:\text{Cs}^+$ as the A-cation) is presented according to the formula $\text{Rb}_x\text{Cs}_{1-x}\text{PbX}_3$ (x values = 0, 0.2, 0.4, 0.6, 0.8, 1; $X = \text{Cl}, \text{Br}, \text{I}$). The effective ionic radii were taken from the work of Shannon,²⁶ considering the coordination number of the ions. For the cubic perovskite, the coordination number of the metal and the halide is 6 and for the cation it is 12. Here, we assumed that the structural distortion reduced the symmetry of the structure and the coordination number of the cation as well, from 12 to 8, as suggested by another paper.²⁷ Thus, the used effective ionic radii are Cs^+ (1.74 Å), Rb^+ (1.61 Å), Pb^{2+}

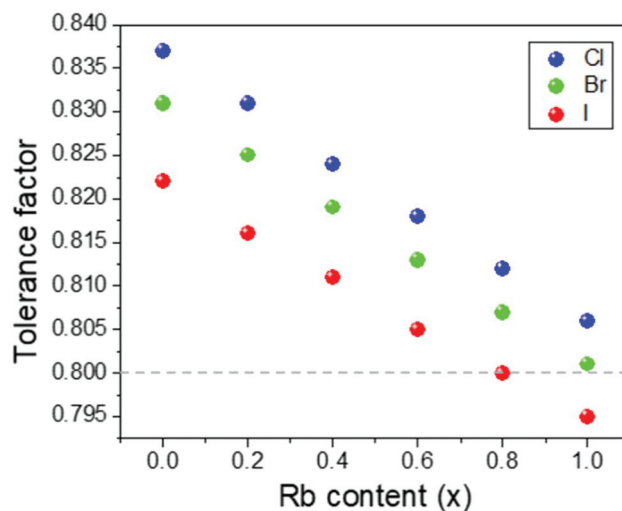


Fig. 1 The calculated tolerance factors of $\text{Rb}_x\text{Cs}_{1-x}\text{PbX}_3$ ($X = \text{Cl}, \text{Br}, \text{I}$) perovskites as a function of the Rb content (x), ranges from $x = 0$ to $x = 1$. The grey dashed line represents the bottom limit of the empirical formability range of the perovskite (0.8).

(1.19 Å), Cl^- (1.81 Å), and Br^- (1.96 Å). More details are found in Table S1 in the ESI.† The graph shows a linear relationship between the TF and the Rb^+ content and suggests that some compositions are expected to form a perovskite structure. When the Rb^+ content is higher, the TF is smaller. The dashed line represents the bottom limit of the perovskite formability range. According to the calculated TFs, the perovskite crystal structure can be formed while x equals 0.0–1.0 for Cl and Br, and 0.0–0.6 for I, revealing that Cl- and Br-based perovskites have a higher chance to form the perovskite with a higher Rb^+ content. A recent work by Linaburg *et al.* was focused on the size of the A-cation in bulk mixed-cation perovskites and how it affects their properties.¹³ This work suggested that the Rb^+ -based perovskite crystal structure is unstable at room temperature, leading to lattice deformations that result in other Rb^+ -based phases. It is reasonable to assume that the intrinsic strains inside the lattice in the bulk differ from those in the nano-size. Therefore, it is expected that nano-sized particles would provide a more adaptive nature with A-cation substitutions.^{19,24} This graph gives a prediction for the probability to form Rb-based perovskite from a theoretical point of view, yet it cannot assure the formation of a stable perovskite in the nominal ratios, which is also different in the bulk and the nano-scale.

In this work, we successfully demonstrate the possibility of introducing a Rb^+ cation with a Cs^+ cation in $\text{Rb}_x\text{Cs}_{1-x}\text{PbX}_3$ NPs using a hot injection method.¹⁶ Briefly, the Rb^+/Cs^+ -oleate precursor was prepared by mixing $\text{Rb}_2\text{CO}_3/\text{Cs}_2\text{CO}_3$ or a mix of them in a 3-neck flask along with oleic acid (OA) and octadecene (ODE). For the lead halide (PbX_2 ; $X = \text{Cl}, \text{Br}$) precursor, PbCl_2 or PbBr_2 was loaded in an additional 3-neck flask along with OA, oleylamine (OLA), and ODE. In the case of PbCl_2 , trioctylphosphine (TOP) was added for a complete dissolution

of the salt. Both flasks were degassed under vacuum, and then the temperature was increased to 150 °C for the reaction. A desired volume of Rb^+/Cs^+ -oleate was swiftly injected to the PbX_2 flask. After ~ 5 seconds, an ice bath was applied to quench the reaction. The crude NPs were purified through centrifugation, with isopropanol as an anti-solvent, for further characterization.

Fig. 2 presents the absorption and photoluminescence (PL) spectra of the different mixed-cation perovskite NPs with chloride ($\text{Rb}_x\text{Cs}_{1-x}\text{PbCl}_3$, Fig. 2a and b) and bromide ($\text{Rb}_x\text{Cs}_{1-x}\text{PbBr}_3$, Fig. 2c and d). The x values correspond to 0, 0.2, 0.4, 0.6, and 0.8. Clearly, there is a blue shift in absorption and PL towards shorter wavelengths for both chloride and bromide. The NPs with variable $\text{Rb}^+:\text{Cs}^+$ ratios showed an absorption shift of 0.13 eV and 0.07 eV, respectively. The absorption spectra in Fig. 2a and c confirm that at a higher Rb^+ content, the absorption onset shifts to shorter wavelengths, while the PL peaks shift in the same trend (Fig. 2b and d). The PL derived from the decay of excited mode to the zero-state after excitation, from the conduction band to the valence band. It should be noted that there is no PL peak for $x = 0.8$ in the Cl case due to weak sensitivity of the detector in the near UV spectral region. The mixed cation Rb^+/Cs^+ NPs with iodide as the halide were synthesized and found to be unstable, also showing no optical shift, as shown in Fig. S1 in the ESI.† According to the literature, band-gap tuning was commonly carried out using mixed-halide systems, however mixed-cation systems also affected the band-gap. Many reports on mixed-halide systems and halide-exchange reactions showed a significant optical tuning of perovskite NPs that can be applied to various utilizations.^{16–18} Substitutions of the halides influence the electronic and

optical properties by changing the energy level of the valence band as a result of different energies of their p orbitals, thus modifying the band-gap.^{28,29} The substitution of the A-cation influences the band-gap indirectly, through structural distortions. As the A-cation size decreases, the Pb-X-Pb angle is more distorted (whether it is larger or smaller than the ideal 180° angle) and the octahedral tilting is larger. This implies that the overlap of the anti-bonding orbitals of the Pb^{2+} metal cation and the halide anion is deformed compared to the ideal cubic perovskite structure. The energies of the valence band and the conduction band shift upward, the anti-bonding interaction is weaker, and therefore the Pb-X bonds become more stable.^{16,30} This explains why the energy level of the valence band shifts downward, overall widening the band-gap and shifting the absorption to shorter wavelengths.

The synthesis of $x = 1$ (Rb^+ alone as the A-cation) was also implemented with Cl and Br. Cl-Based NPs resulted in another phase of $\text{Rb}_6\text{Pb}_5\text{Cl}_{16}$, which presented a remarkable blue shift towards an onset of ~ 305 nm (Fig. S2 in the ESI†) as reported earlier.²⁵ In the Br case no NPs were formed. Presumably, the perovskite phase was unstable under these conditions. Previous papers report that the RbPbX_3 phase can be stabilized only at elevated temperatures (above 320 °C), which explain the results.^{31–35}

Fig. 3a shows that the NCs exhibit relatively high PLQYs, which are similar to the ones reported for CsPbX_3 ($X = \text{Cl}, \text{Br}$) NCs. It is difficult to distinguish whether there is a pronounced trend while increasing the ratio of $\text{Rb}^+:\text{Cs}^+$. Moreover, the PLQY strongly depends on the purification process of the NPs and the conditions of each synthesis. Moreover, these results suggest that the addition of Rb^+ maintains the good PLQY of the CsPbBr_3 NPs.

Fig. 3b demonstrates the bright PL of the obtained Br-based NPs under UV light, showing green and turquoise-blue emissions for low and high Rb^+ contents, respectively. The change in the $\text{Rb}^+:\text{Cs}^+$ ratio is small, therefore only extreme ratios are presented in this photograph. The emission of the Cl-based NPs is in the near UV spectral range, so the change in the emission colors of the NPs with different Rb^+ contents is indistinguishable by the human eye. The influence of adding

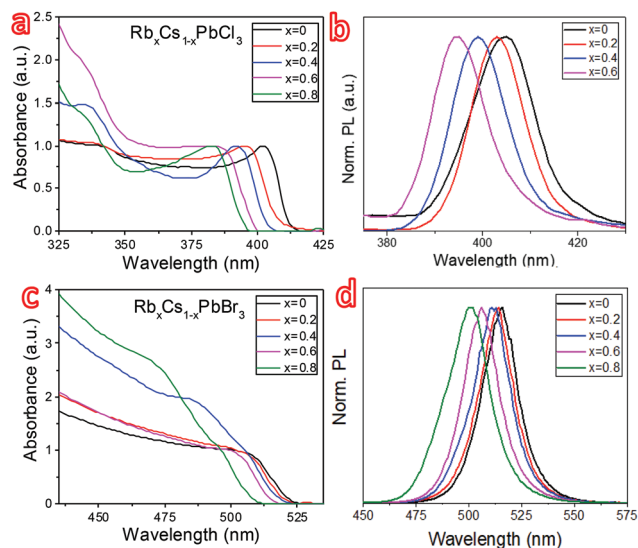


Fig. 2 (a, b) Absorbance and normalized photoluminescence (PL) spectra of $\text{Rb}_x\text{Cs}_{1-x}\text{PbCl}_3$ NPs ($x = 0, 0.2, 0.4, 0.6, 0.8$). (c, d) Absorbance and normalized PL spectra of $\text{Rb}_x\text{Cs}_{1-x}\text{PbBr}_3$ NPs ($x = 0, 0.2, 0.4, 0.6, 0.8$).

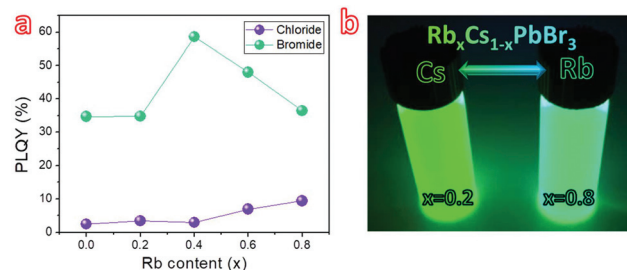


Fig. 3 (a) Photoluminescence quantum yield (PLQY) of the NPs with Cl (purple) and Br (green). (b) Photographs of dispersions of $x = 0.2$ and $x = 0.8$ (left and right vials respectively) samples under ultra-violet light ($\lambda = 365$ nm) show the fluorescence for the extreme molar ratios of Br-based NPs.

Rb⁺ to Cs-based perovskite NPs is unequivocal in this photograph, visualizing optical measurements (Fig. 2).

The crystal structures of Rb_xCs_{1-x}PbX₃ ($x = 0, 0.2, 0.4, 0.6, 0.8, 1$; X = Cl, Br) NPs were measured by powder X-ray diffraction (PXRD) and the results are presented in Fig. 4. The diffractograms show that in both cases, a perovskite crystal structure was detected for low Rb⁺ content. In Fig. 4a, $x = 0$ is characterized with peaks that correspond to an orthorhombic CsPbCl₃ perovskite structure. A cubic structure was also fit to the observed peaks, however, it was previously reported that CsPbCl₃ has an orthorhombic symmetry.¹³ Higher Rb⁺ contents of $x = 0.2$ and $x = 0.4$ resulted in the same CsPbCl₃ perovskite peaks. The observed slight shift of the perovskite peaks is associated with small changes in the values of the unit cell parameters upon Rb–Cs substitution. On a further increase in the Rb⁺ content, the set of perovskite peaks became weaker, and additional peaks had emerged. For example, at $x = 0.6$ and $x = 0.8$ the peaks of the RbPb₂Cl₅ phase were detected (see Fig. S2c†) while at $x = 0.8$ the peaks of the orthorhombic perovskite were absent. Finally, the product of $x = 1$ presented a different set of peaks, which

correspond to a tetragonal Rb₆Pb₅Cl₁₆ phase rather than a perovskite RbPbCl₃ phase, as mentioned earlier.

The synthesis of Rb₆Pb₅Cl₁₆ NPs has been recently published by us.²⁵ These observations indicate a change in the crystal structure triggered by replacing the Cs⁺ cation with the smaller Rb⁺ cation in the lattice, supporting the optical measurements that indicated mixed Rb⁺/Cs⁺ perovskite NPs. It can be assumed that a further increase in the Rb⁺ content, at the expense of Cs⁺, disrupts the perovskite stabilization due to geometrical considerations of the cationic radii. More details about the detected phases in each ratio are given in Table S2 (ESI section†).

In Fig. 4b, the obtained peaks for $x = 0$ correspond to an orthorhombic CsPbBr₃ perovskite structure. Low Rb⁺ contents showed the same perovskite crystal structure, excluding the $x = 0.2$ case, in which two intense peaks are observed. These peaks may relate to the impurities of the Cs₄PbBr₆ phase that is characterized by peaks in the angles 12.8 and 25.9 that can correspond to the observed peaks. In the cases of $x = 0.6$ and $x = 0.8$, the peaks of Rb₄PbBr₆ and RbPb₂Br₅ phases were observed (see Table S2† for more details). According to the literature,

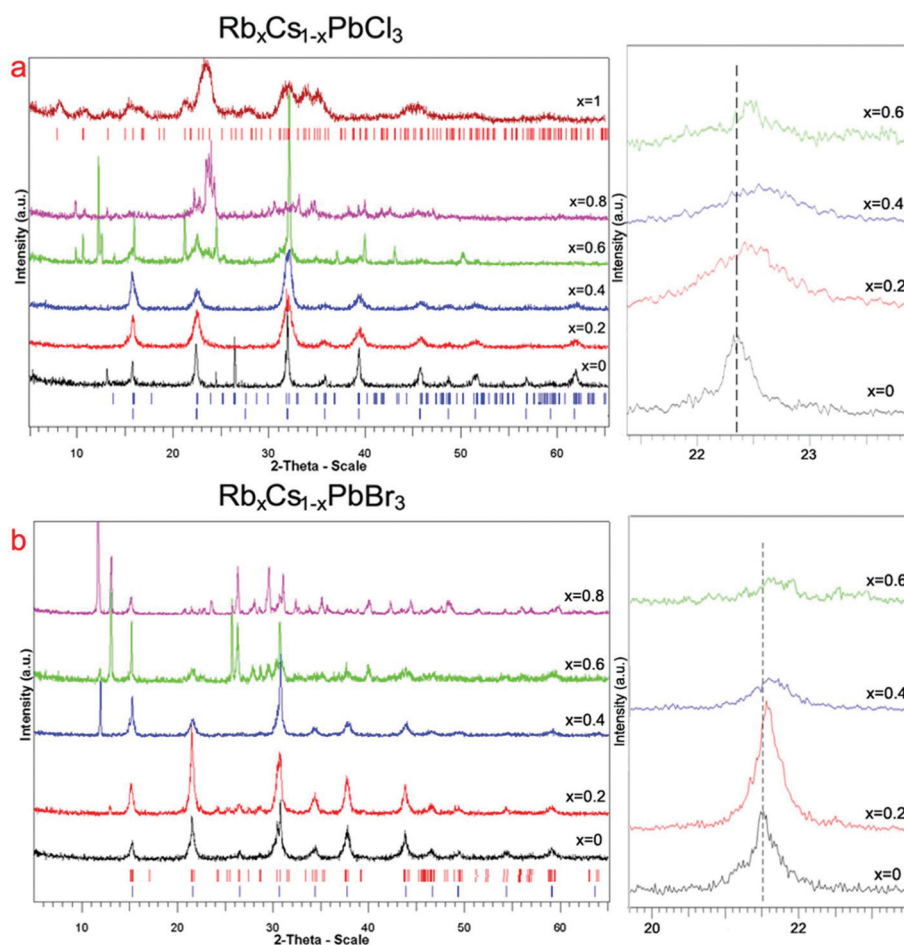


Fig. 4 (a) Powder X-ray diffraction (PXRD) patterns for Rb_xCs_{1-x}PbCl₃ ($x = 0$ to $x = 1$) NPs. (b) PXRD patterns for Rb_xCs_{1-x}PbBr₃ ($x = 0$ to $x = 0.8$) NPs. Theoretical peak positions of orthorhombic and cubic (for comparison) CsPbCl₃ (a), CsPbBr₃ (b) and tetragonal Rb₆Pb₅Cl₁₆ phases (top of (a)) are shown by vertical bars, on the right are zoomed fragments of XRD patterns.

the Rb_4PbBr_6 phase was previously obtained using solid state reactions, starting from binary precursors.³⁶ The possibility of the presence of a small impurity of additional phases ($\text{Rb}_6\text{Pb}_5\text{Cl}_{16}$, RbPb_2Cl_5 , Rb_2PbCl_4 , Rb_3PbCl_5 , and RbPb_2Br_5) in the synthesized material is also noted by other reports. From the phase diagram reported by Monzel *et al.*³⁵ a 1 : 1 mixture (*i.e.* RbPbCl_3) will not form a single perovskite phase at room temperature but instead it will form a two-phase mixture. In this work, this phase was proved to crystallize in a rhombohedral K_4CdCl_6 -type structure in contrast to an earlier paper, which suggested a tetragonal Tl_4HgBr_6 -type structure.³⁷ Minimizing the structure to the nano-scale, here the PXRD results showed a tetragonal Rb_4PbBr_6 structure in $x = 0.6$ and $x = 0.8$ products. The reasons to declare one phase over the other are stability-related. It was concluded that only ns^2 -type of A-cations (such as In^+ and Tl^+) can stabilize the tetragonal Tl_4HgBr_6 -type structure due to polarization effects and high electronegativity, compared with alkali ions of comparable size, such as Rb^+ . Possibly, a much “looser” crystal structure is formed in the nano-scale, which contributes to the formability of the less-preferred structure type.^{37,38}

More concisely, there is a gradual process of phase modifications in both Cl- and Br-based NPs with an increase in the amount of Rb^+ (over Cs). It occurs due to octahedral tilting, and when the octahedral tilting is large, a more stable crystal phase is formed until the perovskite crystal structure is lost completely (for example in Cl; where $x = 1$). In the case of Br-based NPs, the NP formation was restricted to a maximal ratio of $x = 0.8$, which is unable to form a stable perovskite structure with Rb^+ alone.

Fig. 5 depicts transmission electron microscopy (TEM) images of the different NPs with a square shape. Size distributions of each product, with different Rb^+ contents, were measured using ImageJ software (Fig. S3 in the ESI†). Accordingly, Fig. S3† presents the size distributions and the average side length of the NCs, assuming a square shape. The size distributions along with the average side lengths of the NPs show a declining trend with an increase of the Rb^+

content for both Cl and Br. Upon adding more rubidium to the crystal, at the expense of cesium, *d*-spacing among the crystallographic plains decreases because Rb^+ is smaller than Cs^+ , affecting the average size of the NPs. One can wonder if the optical blue shifts of the NPs with an increase in Rb^+ content originate from quantum confinement rather than octahedral tilting. It was suggested that the influence of substituting the monovalent cation depends on the crystalline symmetry of the system.³⁹ If the starting perovskite phase is cubic, replacing the original cation results in a change in the lattice parameters, and therefore expansion or contraction of the lattice occurs. If the starting system is tetragonal or orthorhombic, the A-cation substitution shows two competing effects regarding both the crystal size and tilting angles of the octahedra. On the one hand, the smaller A-cation can cause the lattice to shrink, thus strengthen the antibonding overlap between X-p and Pb-s orbitals. On the other hand, the small A-cation increases the Pb–X–Pb angle, and thus weakens the p–s overlap. Simulations by Meloni *et al.* determined that typically the second effect dominates, overall lowering the conduction band and increasing the band-gap.³⁹ We conclude that both effects occur, but the contraction of the lattice upon Rb^+ addition will not cause quantum confinement because the average size is above the Bohr diameter of the NPs, which is 5 nm and 7 nm for CsPbCl_3 and CsPbBr_3 respectively.¹⁹ Therefore, the optical change is associated with the octahedral tilting.

Furthermore, a control experiment was performed in order to ensure that the addition of Rb^+ causes the changes in the optical properties. $\text{Cs}_{0.2}\text{PbBr}_3$, $\text{Cs}_{0.4}\text{PbBr}_3$ and $\text{Cs}_{0.8}\text{PbBr}_3$ without Rb^+ were synthesized (importantly, these chemical formulas indicate the composition at the preparation of the solution, which emphasize that no Rb^+ was used), and their absorption spectra were compared to the corresponding absorption of the syntheses with Rb^+ (*i.e.* $\text{Cs}_{0.2}\text{Rb}_{0.8}\text{PbBr}_3$, $\text{Cs}_{0.4}\text{Rb}_{0.6}\text{PbBr}_3$ and $\text{Cs}_{0.8}\text{Rb}_{0.2}\text{PbBr}_3$ as shown in Fig. 6). It can be seen from Fig. 6d that changing the Cs concentration results in a shift of the absorption, however Fig. 6a, b and c

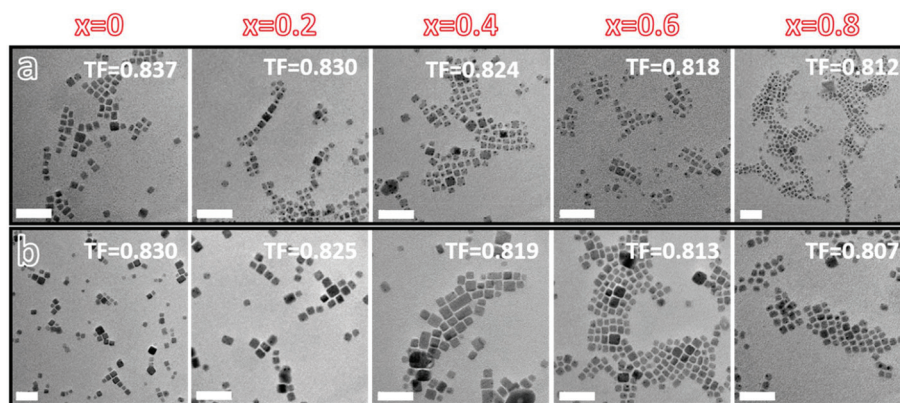


Fig. 5 (a) Transmission electron microscopy (TEM) images of $\text{Rb}_x\text{Cs}_{1-x}\text{PbCl}_3$ ($x = 0, 0.2, 0.4, 0.6, 0.8$) NPs with the corresponding tolerance factors (TF). (b) TEM images of $\text{Rb}_x\text{Cs}_{1-x}\text{PbBr}_3$ ($x = 0, 0.2, 0.4, 0.6, 0.8$) NPs with the corresponding TF. The scale bars correspond to 50 nm.

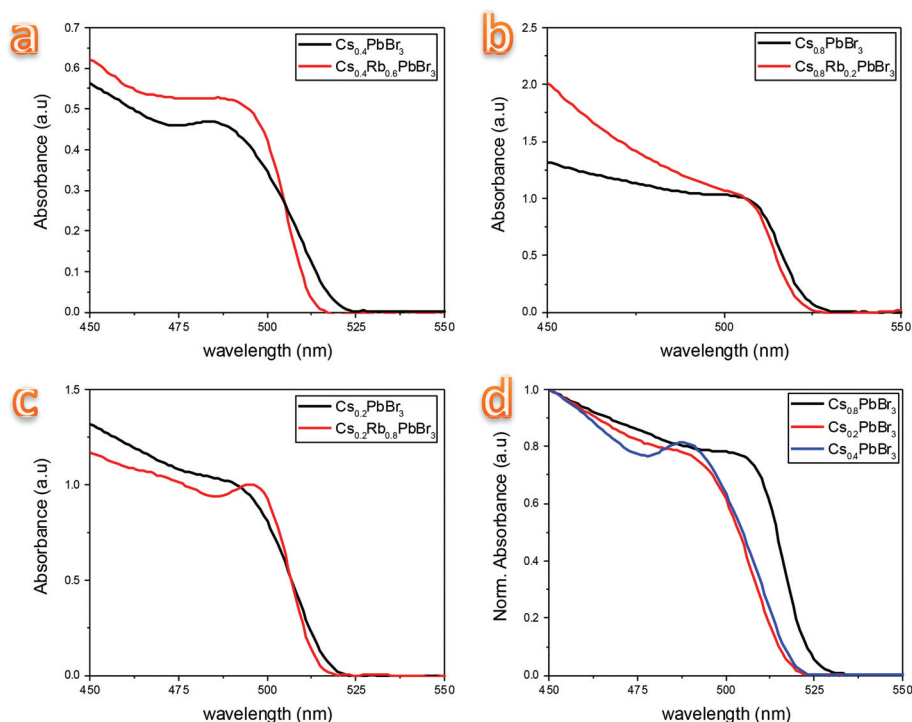


Fig. 6 (a) Absorbance of $\text{Cs}_{0.2}\text{PbBr}_3$ and $\text{Cs}_{0.2}\text{Rb}_{0.8}\text{PbBr}_3$. (b) Absorbance of $\text{Cs}_{0.4}\text{PbBr}_3$ and $\text{Cs}_{0.4}\text{Rb}_{0.6}\text{PbBr}_3$. (c) Absorbance of $\text{Cs}_{0.2}\text{PbBr}_3$ and $\text{Cs}_{0.2}\text{Rb}_{0.8}\text{PbBr}_3$. (d) Absorbance of $\text{Cs}_{0.2}\text{PbBr}_3$, $\text{Cs}_{0.4}\text{PbBr}_3$ and $\text{Cs}_{0.8}\text{PbBr}_3$.

show that when Rb^+ is added to the NPs the absorption spectra are further blue shifted compared to without Rb^+ . This provides an additional confirmation that the optical changes are a result of the presence of Rb in the NPs. An XRD measurement of $\text{Cs}_{0.2}\text{PbBr}_3$ also shows that the perovskite in the orthorhombic phase is formed in this case although a reduced amount of Cs is used in the synthesis (see Fig. S7 in the ESI†). It can be concluded that the amount of Cs in the synthesis affects mainly the amount of the NPs which are formed.

Apart from the size, the shape also becomes less defined with a higher Rb^+ content. It can be related to the change in the crystal phase that may occur due to serious deformations of the perovskite phase into a mix of Cs^+ and Rb^+ -based phases, as the PXRD confirms.

Moreover, black dots appear in all the images. A recent work investigated this issue thoroughly and showed that the black dots are Pb^0 seeds that nucleate prior to the reaction in the PbX_2 flask. According to these findings, the use of Rb^+ in the same molar ratio as its Cs^+ counterpart is probably insufficient for a complete crystallization, and thus more Pb^0 seeds appear at higher Rb^+ concentrations.⁴⁰

Energy dispersive X-ray spectroscopy (EDS) was used to obtain an estimation of the elemental composition of the NPs. These measures were collected in scanning transmission electron microscopy (STEM) mode. EDS quantification data for $x = 0.8$, for both Cl and Br products, are found in Fig. S4, and S5† and confirm that the NPs are composed of Rb, Cs, Pb, and Cl/Br. In the case of $\text{Rb}_{0.8}\text{Cs}_{0.2}\text{PbCl}_3$, the atomic ratios are 19.14 (Rb), 12.83 (Cs), 38.98 (Pb), and 29.04 (Cl). The atomic ratio

between Rb and Cs do not agree with the expectation of 1 : 4 based on the molar ratio, yet there is more Rb than Cs in the examined NPs. The ratio between Rb/Cs (as the A-cation) and Pb is 1.2, which is close to the expected ratio (1 : 1). The atomic percentage of Cl deviates from the anticipated content, which is supposed to be three times larger than Rb/Cs or Pb according to the ABX_3 formula. However, Cs-based inorganic perovskite NPs are known to quickly degrade during TEM and STEM analysis because of the electron beam. In the case of Br, the atomic percentage of Rb/Cs together is lower than expected and differs from the Cl-based NPs. Unexpectedly, the Cs content is higher than the Rb content. In addition, the atomic contents of Br and Pb are 60.39% and 23.98% respectively, which meet the expectations. We can predict the following; (1) Cl evaporated as Cl_2 during the measurement and this can result in the de-stabilization of the perovskite structure. Therefore, Pb^{2+} cations can undergo reduction by the energized electrons of the beam. (2) In Br-based perovskite NPs, the Rb^+ effect is less on the crystal. This conclusion agrees with the milder change in absorption while adding more Rb^+ , in contrast to Cl-based perovskite NPs. It is also supported by the calculated TF (Fig. 1) for Br-based perovskite NPs, which are less stable with the increase in the Rb^+ content compared to Cl-based perovskite NPs. It is important to note that the nominal ratios between Cs^+ and Rb^+ are theoretical and are limited in predicting the real ratios in the as-synthesized NPs.

The stability of the NPs was measured by tracking the absorption of the NPs once a week for a whole month. All NPs showed a red shift in absorption in the first week after the syn-

thesis. No more changes in the absorption were observed afterwards (Fig. S6†).

The chloride NPs were less stable as the absorption spectra of the different concentrations were merged together after the first week while the bromide based NPs maintain the difference in the absorption spectra for the whole month.

Experimental

Chemicals

Cesium carbonate (Cs_2CO_3 , 99.9%, Sigma-Aldrich), rubidium carbonate (Rb_2CO_3 , 99%, Sigma-Aldrich), lead(II) chloride (PbCl_2 , 98%, Sigma-Aldrich), lead(II) bromide (PbBr_2 , $\geq 98\%$, Sigma-Aldrich), oleic acid (OA, 90%, Sigma-Aldrich), oleylamine (OLAM, 70%, Sigma-Aldrich), trioctylphosphine (TOP, 97%, Strem), 1-octadecene (ODE, 90%, Sigma-Aldrich), 2-propanol ($\geq 99.8\%$, Sigma-Aldrich), and hexane (not pure, Gadot) were purchased and used as received, without any further purification.

Preparation of Rb/Cs-oleate

The Rb/Cs-oleate precursor was prepared according to a previously published procedure by Protesescu *et al.*¹⁶ Different molar ratios of $\text{Cs}_2\text{CO}_3/\text{Rb}_2\text{CO}_3$ (total of 1.228 mmol) were mixed with 625 μL of oleic acid (OA) and 7.5 mL of 1-octadecene (ODE) in a 50 mL 3-neck flask. The solution was degassed for 1 h under vacuum conditions at 120 °C and then heated to 150 °C under an Ar flow.

Synthesis of $\text{Rb}_x\text{Cs}_{1-x}\text{PbX}_3$ (X = Cl, Br) NPs

The NPs were synthesized according to Protesescu *et al.* 0.188 mmol of PbX_2 were mixed with 0.5 mL of OA, 0.5 mL of OLA, and 5 mL of ODE in an additional 100 mL 3-neck flask. 1 mL of TOP was added in the case of PbCl_2 . The solution was degassed for 1 h under vacuum at 120 °C and then heated to 150 °C under an argon flow. The reaction was carried out by the injection of 0.4 mL of the Rb/Cs-oleate precursor solution into the PbX_2 precursor solution using a preheated syringe. The reaction was quenched using an ice bath after a few seconds. The crude solution was centrifuged at 8000 rpm for 10 min. Isopropanol was added in a volume ratio of 1 : 1 and the NPs were centrifuged again at 6000 rpm for 10 min. The purified NPs were dispersed in hexane for further characterization.

High resolution transmission electron microscopy (HRTEM)

Morphology and elemental composition of the NPs were analyzed with a HR (S)TEM (High Resolution Scanning Transmission Electron Microscope) Tecnai F20 G2 (FEI Company, USA). Sample preparation was performed as follows: 3.5 μL of the NP dispersion were dropped on a copper grid coated with an amorphous carbon film, and then the solvent was evaporated using a vacuum chamber. Elemental analysis of NPs was performed with EDAX EDS (Energy Dispersive

X-Ray Spectroscopy) when the microscope was operated in STEM mode at an accelerating voltage of 200 kV.

Powder X-ray diffraction (PXRD)

Powder X-ray diffraction measurements were performed using a D8 Advance Diffractometer (Bruker AXS, Karlsruhe, Germany) with a goniometer radius of 217.5 mm, a secondary graphite monochromator, 2° Soller slits, and a 0.2 mm receiving slit. XRD patterns within the range of 3–60° 2θ were recorded at room temperature using $\text{CuK}\alpha$ radiation ($\lambda = 1.5418 \text{ \AA}$) with the following measurement conditions: tube voltage of 40 kV, tube current of 40 mA, step-scan mode with a step size of 0.02° 2θ , and counting time of 1–3 s per step. The value of the grazing incidence angle was 2.5°.

Optical measurements

Absorption spectra were recorded using a Jasco V-670 spectrophotometer. Photoluminescence (PL) measurements were performed using an L-shaped spectrofluorometer (Edinburgh Instruments FL920). The Cl- and Br-based NPs were excited at 320 and 400 nm respectively. The emission was collected at 90° in the range of 350–440 nm for Cl and 450–550 nm for Br. Photoluminescence quantum yields (PLQY) were measured using a Hamamatsu absolute PLQY spectrometer C11347.

Conclusions

This paper describes the introduction of Rb^+ cations into CsPbX_3 NPs. The addition of a small amount of Rb^+ cation in increasing ratios affects the levels of structural pressure on the inorganic CsPbX_3 (X = Cl, Br) perovskite NPs. $\text{Rb}_x\text{Cs}_{1-x}\text{PbX}_3$ (X = Cl, Br) systems were recently reported for solid solutions and found to have tunable optical properties. This was explained by an increase in octahedral tilting, which affects the anti-bonding overlap of the Pb^{2+} and the X^- orbitals.¹³ However, in this paper the synthesis and characterization of $\text{Rb}_x\text{Cs}_{1-x}\text{PbX}_3$ NPs were developed to have more comprehensive knowledge about the structural and optical consequences of A-cation modifications in the nano-scale, which opens a window for high structural flexibility. The obtained NPs were characterized and found to exhibit high PLQYs, which are comparable to those of the original CsPbX_3 nanoparticles. In addition, the band-gaps of Cl- and Br-based NPs could be enlarged by increasing the amount of Rb^+ in the crystal. TEM images showed square-shaped NPs and EDS elemental analysis confirmed the presence of Rb^+ in the NPs. Although calculations of the tolerance factors of these NPs predicted that high contents of Rb^+ yield are close to the lower limit of the perovskite formability range that can lead to unstable perovskites, the results proved that mixed-cation perovskite NPs are indeed formed, possessing properties that are very similar to the known CsPbX_3 NPs. The possibility to obtain a mild band-gap tuning for Rb^+/Cs^+ mixed-cation NPs is one step forward to a complete understanding of perovskite nanostructures. Future experiments can be attributed to apply these NPs for

light emitting devices or as thin films that may enhance the performance of perovskite solar cells.

Conflicts of interest

There are no conflicts to declare.

Acknowledgements

This work was supported by the Israel ministry of energy and the Israel ministry of the chief scientist.

References

- C. C. Stoumpos, C. D. Malliakas and M. G. Kanatzidis, Semiconducting tin and lead iodide perovskites with organic cations: phase transitions, high mobilities, and near-infrared photoluminescent properties, *Inorg. Chem.*, 2013, **52**(15), 9019–9038.
- J. H. Noh, S. H. Im, J. H. Heo, T. N. Mandal and S. Il Seok, Chemical management for colorful, efficient, and stable inorganic–organic hybrid nanostructured solar cells, *Nano Lett.*, 2013, **13**(4), 1764–1769.
- F. Hao, C. C. Stoumpos, R. P. H. Chang and G. Mercuri, Kanatzidis. Anomalous band gap behavior in mixed Sn and Pb perovskites enables broadening of absorption spectrum in solar cells, *J. Am. Chem. Soc.*, 2014, **136**(22), 8094–8099.
- M. R. Filip, G. E. Eperon, H. J. Snaith and F. Giustino, Steric engineering of metal-halide perovskites with tunable optical band gaps, *Nat. Commun.*, 2014, **5**(5757), 1–9.
- A. Amat, E. Mosconi, E. Ronca, C. Quarti, P. Umari, Md K. Nazeeruddin, M. Grätzel and F. De Angelis, Cation-induced band-gap tuning in organohalide perovskites: interplay of spin–orbit coupling and octahedra tilting, *Nano Lett.*, 2014, **14**(6), 3608–3616.
- C. C. Stoumpos, L. Frazer, D. J. Clark, Y. S. Kim, S. H. Rhim, A. J. Freeman, J. B. Ketterson, J. I. Jang and M. G. Kanatzidis, Hybrid germanium iodide perovskite semiconductors: active lone pairs, structural distortions, direct and indirect energy gaps, and strong nonlinear optical properties, *J. Am. Chem. Soc.*, 2015, **137**(21), 6804–6819.
- W. Liu, Q. Lin, H. Li, K. Wu, I. Robel, J. M. Pietryga and V. I. Klimov, Mn²⁺-Doped lead halide perovskite nanocrystals with dual-color emission controlled by halide content, *J. Am. Chem. Soc.*, 2016, **138**(45), 14954–14961.
- D. Parobek, B. J. Roman, Y. Dong, Ho Jin, E. Lee, M. Sheldon and D. H. Son, Exciton-to-dopant energy transfer in Mn-doped cesium lead halide perovskite nanocrystals, *Nano Lett.*, 2016, **16**(12), 7376–7380.
- H. Liu, Z. Wu, J. Shao, D. Yao, H. Gao, Yi Liu, W. Yu, H. Zhang and B. Yang, CsPb_xMn_{1-x}Cl₃ Perovskite Quantum Dots with High Mn Substitution Ratio, *ACS Nano*, 2017, **11**(2), 2239–2247.
- T. Duong, H. K. Mulmudi, H. Shen, Y. L. Wu, C. Barugkin, Y. O. Mayon, H. T. Nguyen, *et al.*, Structural engineering using rubidium iodide as a dopant under excess lead iodide conditions for high efficiency and stable perovskites, *Nano Energy*, 2016, **30**, 330–340.
- T. Duong, Yi L. Wu, H. Shen, J. Peng, X. Fu, D. Jacobs, E.-C. Wang, *et al.*, Rubidium Multication Perovskite with Optimized Bandgap for Perovskite-Silicon Tandem with over 26% Efficiency, *Adv. Energy Mater.*, 2017, **7**, 1700228.
- M. Saliba, T. Matsui, K. Domanski, Ji.-Y. Seo, A. Ummadisingu, S. M. Zakeeruddin, J.-P. Correa-Baena, *et al.*, Incorporation of rubidium cations into perovskite solar cells improves photovoltaic performance, *Science*, 2016, **354**(6309), 206–209.
- M. R. Linaburg, E. T. McClure, J. D. Majher and P. M. Woodward, Cs_{1-x}Rb_xPbCl₃ and Cs_{1-x}Rb_xPbBr₃ Solid Solutions: Understanding Octahedral Tilting in Lead Halide Perovskites, *Chem. Mater.*, 2017, **29**(8), 3507–3514.
- <https://www.nrel.gov/pv/assets/images/efficiency-chart.png> (24.12.17).
- W. S. Yang, B.-W. Park, E. H. Jung, N. J. Jeon, Y. C. Kim, D. Uk Lee, S. S. Shin, *et al.*, Iodide management in formamidinium-lead-halide-based perovskite layers for efficient solar cells, *Science*, 2017, **356**(6345), 1376–1379.
- L. Protesescu, S. Yakunin, M. I. Bodnarchuk, F. Krieg, R. Caputo, C. H. Hendon, R. Xi Yang, A. Walsh and M. V. Kovalenko, Nanocrystals of cesium lead halide perovskites (CsPbX₃, X = Cl, Br, and I): novel optoelectronic materials showing bright emission with wide color gamut, *Nano Lett.*, 2015, **15**(6), 3692–3696.
- G. Nedelcu, L. Protesescu, S. Yakunin, M. I. Bodnarchuk, M. J. Grotevent and M. V. Kovalenko, Fast anion-exchange in highly luminescent nanocrystals of cesium lead halide perovskites (CsPbX₃, X = Cl, Br, I), *Nano Lett.*, 2015, **15**(8), 5635–5640.
- Q. A. Akkerman, V. D’Innocenzo, S. Accornero, A. Scarpellini, A. Petrozza, M. Prato and L. Manna, Tuning the optical properties of cesium lead halide perovskite nanocrystals by anion exchange reactions, *J. Am. Chem. Soc.*, 2015, **137**(32), 10276–10281.
- L. Protesescu, S. Yakunin, S. Kumar, J. Bär, F. Bertolotti, N. Masciocchi, A. Guagliardi, *et al.*, Dismantling the “Red Wall” of Colloidal Perovskites: Highly Luminescent Formamidinium and Formamidinium–Cesium Lead Iodide Nanocrystals, *ACS Nano*, 2017, **11**(3), 3119–3134.
- V. M. Goldschmidt, Die gesetze der krystallochemie, *Naturwissenschaften*, 1926, **14**(21), 477–485.
- G. Kieslich, S. Sun and A. K. Cheetham, An extended tolerance factor approach for organic–inorganic perovskites, *Chem. Sci.*, 2015, **6**(6), 3430–3433.
- W. Travis, E. N. K. Glover, H. Bronstein, D. O. Scanlon and R. G. Palgrave, On the application of the tolerance factor to inorganic and hybrid halide perovskites: a revised system, *Chem. Sci.*, 2016, **7**(7), 4548–4556.

- 23 M. A. Green, A. Ho-Baillie and H. J. Snaith, The emergence of perovskite solar cells, *Nat. Photonics*, 2014, **8**(7), 506–514.
- 24 He Huang, M. Bodnarchuk, S. V. Kershaw, M. V. Kovalenko and A. L. Rogach, Lead Halide Perovskite Nanocrystals in the Research Spotlight: Stability and Defect-Tolerance, *ACS Energy Lett.*, 2017, **2**, 2071–2083.
- 25 D. Amgar, M. Wierzbowska, V. Uvarov, V. Gutkin and L. Etgar, Novel rubidium lead chloride nanocrystals: synthesis and characterization, *Nano Futures*, 2017, **1**, 021002.
- 26 R. D. Shannon, Revised effective ionic radii and systematic studies of interatomic distances in halides and chalcogenides, *Acta Crystallogr., Sect. A: Cryst. Phys., Diffraction, Theor. Gen. Crystallogr.*, 1976, **32**(5), 751–767.
- 27 R. H. Mitchell, M. D. Welch and A. R. Chakhmouradian, Nomenclature of the perovskite supergroup: A hierarchical system of classification based on crystal structure and composition, *Mineral. Mag.*, 2017, **81**(3), 411–461.
- 28 Y. H. Chang, C. H. Park and K. Matsuishi, First-Principles Study of the Structural and the Electronic Properties of the Lead-Halide-Based Inorganic-Organic Perovskites (CH₃NH₃)PbX₃ and CsPbX₃ (X = Cl, Br, I), *J. Korean Phys. Soc.*, 2004, **44**, 889–893.
- 29 K. T. Butler, J. M. Frost and A. Walsh, Band alignment of the hybrid halide perovskites CH₃NH₃PbCl₃, CH₃NH₃PbBr₃ and CH₃NH₃PbI₃, *Mater. Horiz.*, 2015, **2**(2), 228–231.
- 30 G. E. Eperon, S. D. Stranks, C. Menelaou, M. B. Johnston, L. M. Herz and H. J. Snaith, Formamidinium lead trihalide: a broadly tunable perovskite for efficient planar heterojunction solar cells, *Energy Environ. Sci.*, 2014, **7**(3), 982–988.
- 31 K. Treis, Neues Jahrbuch Mineral, *Geol.*, 1914, **37**, 784.
- 32 A. M. Glazer, The classification of tilted octahedra in perovskites, *Acta Crystallogr., Sect. B: Struct. Crystallogr. Cryst. Chem.*, 1972, **28**(11), 3384–3392.
- 33 H. P. Beck, M. Schramm, R. Haberkorn, R. Dinnebier and P. W. Stephens, Synthesis and Crystal Structure of Rb₆Pb₅Cl₁₆, *Z. Anorg. Allg. Chem.*, 1998, **624**, 393–398.
- 34 C. J. Howard and H. T. Stokes, Group-theoretical analysis of octahedral tilting in perovskites, *Acta Crystallogr., Sect. B: Struct. Sci.*, 1998, **54**(6), 782–789.
- 35 H. Monzel, M. Schramm, K. StoÈwe and H. P. Beck, Zur Neuuntersuchung des Phasendiagramms RbCl/PbCl₂, *Z. Anorg. Allg. Chem.*, 2000, **626**(2), 408–411.
- 36 H. P. Beck and W. Milius, Study on A₄BX₆ Compounds. II [1]. Refinement of the Structure of Rb₄PbBr₆ and a Note on the Existence of Rb₄HgI₆ and K₄CdI₆, *Z. Anorg. Allg. Chem.*, 1988, **562**(1), 102–104.
- 37 M. Cola, V. Massarotti, R. Riccardi and C. Sinistri, Binary systems formed by lead bromide with (Li, Na, K, Rb, Cs and Tl) Br: a DTA and diffractometric study, *Z. Naturforsch., A: Astrophys. Phys. Phys. Chem.*, 1971, **26**(8), 1328–1332.
- 38 H. P. Beck and W. Milius, Study on A₄BX₆ Compounds. III [1]. ns² cations as a prerequisite for a structure type and their interaction in ternary halides with the formula type A₄BX₆ (A: In, Tl; B: Cd, Pb, Ge; X: Cl, Br, I), *Z. Anorg. Allg. Chem.*, 1988, **562**(1), 105–114.
- 39 S. Meloni, G. Palermo, N. A. Astani, B. F. E. Curchod, M. Graetzel and U. Roethlisberger, Valence and conduction bands engineering in halide perovskites for solar cell applications, 2014, arXiv preprint arXiv:1412.3659.
- 40 T. Udayabhaskararao, M. Kazes, L. Houben, H. Lin and D. Oron, Nucleation, Growth, and Structural Transformations of Perovskite Nanocrystals, *Chem. Mater.*, 2017, **29**(3), 1302–1308.